

Bam Earthquake Prediction & Space Technology

Zhonghao Shou
Darrell Harrington
Earthquake Prediction Center
500E 63rd 19K, New York, NY 10021
<http://quake.exit.com>

Introduction

The principal application of space technology to earthquake prediction has traditionally been measurements of ground motion. While this approach has contributed significantly to geophysical studies, it has not yet yielded an earthquake prediction method. An alternative approach that has recently shown great promise is satellite imaging of strange non-meteorological cloud formations and their correlation with earthquakes. Shou used such a cloud (see Fig. 1) to predict the Bam earthquake of Dec. 26, 2003 to the public. Coarse and fine predictions were made public on the internet (@1) at 17:58 UTC, Dec. 25, 2003. The fine prediction stated that there would be an earthquake of magnitude more than or equal to 5.5 within 60 days along a fault described in Fig. 1, while the coarse prediction allowed magnitude 5 and above, within 98 days. The Bam earthquake occurred precisely on the predicted fault, and its magnitude was within the predicted magnitude windows.

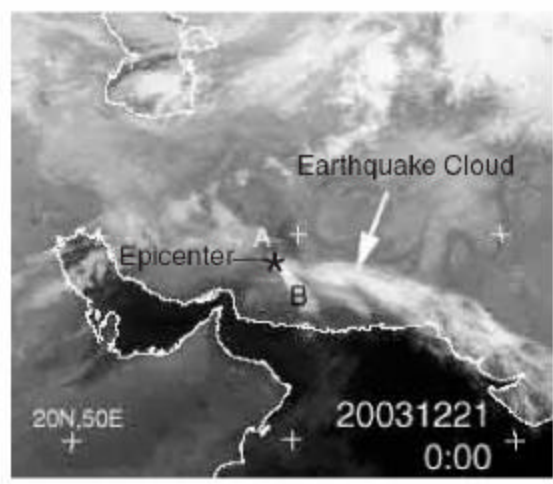


Figure 1. the Bam Earthquake Cloud

This image of IndoEx satellite (@2) shows an earthquake cloud emerging from fault AB on Dec. 21, 2003, marked by a white arrow, by which Shou predicted an M5.5 or bigger earthquake in Fault AB within 60 days on Dec. 25, 2003 to the public (@1). On Dec. 26, an earthquake of 6.8 Ms happened in Bam (28.99N, 58.29E), Iran (marked by *), exactly where the cloud had emerged.

The first known record of this kind of earthquake precursor is the Chronicle of Lon-De County, China, 381 years ago (recompiled in 1935): "It was sunny and warm; the sky was blue and clear. Suddenly, there appeared threads of black clouds spanning the sky like a long snake. The clouds stayed for a long time, so there would be an earthquake" (1). The predicted earthquake was the magnitude 7.0 Guyuan (36.5 N, 106.3 E), Ningxia province earthquake on Oct. 25, 1622. It was the only big one in Western China (< 110 E) within 148 years from Jul. 26, 1561 to Oct. 13, 1709 (2), so this prediction is remarkable.

This method was recently revived in Japan and China. On the morning of Mar. 6, 1978 Kagida, the former mayor of Nara city, Japan, predicted the 7.8 Kantow earthquake on Mar. 7 by the clouds (1). He also proposed that the epicenter of an earthquake would be located in the mid-perpendicular plane of the clouds, which later proved to be incorrect. Following this successful prediction, there was a brief period of activity in the scientific communities in China and Japan. Three kinds of earthquake clouds: rope-shaped, rib-shaped (we denote it wave-shaped), and radiation-shaped, were announced. Unfortunately, the connection between clouds and earthquakes faded from view after 1985.

On the other hand, Shou made his first earthquake prediction in Hangzhou (30.25N, 120.17E), China by a long line-shaped cloud with a tail pointing in the northwest direction on Jun. 20, 1990. 18 hours later, a magnitude 7.7 earthquake struck Iran, and killed or injured 370,000 people. Because the earthquake was the only one bigger than 7 to the northwest of Hangzhou for 333 days from May 31, 1990 to Apr. 28, 1991, He believed that there must be a strong relationship between the cloud and the earthquake. As long as the epicenter was not located by Kagida's law, but on where the cloud's tail pointed toward, He believed that the method of earthquake clouds should not have been abandoned.

Over the last 10 years, with the aid of satellite weather images available on the internet (@ 2-10) Shou has observed similar correlations in sufficient numbers to enable the development of a successful earthquake prediction method. He has used this method to generate 50 independent predictions certified by the United States Geological Survey (USGS), of which 36 were correct. We will describe a model to explain the correlations, a statistical analysis of the set of predictions, and prospects for improving the both precision and reliability of the predictions.

Earthquake Cloud Model

Shou first proposed a model for the formation of earthquake clouds (2). When a huge rock is stressed by external forces, its weak parts break first and small earthquakes occur. For example, the Southern California earthquake data (@11) show that small shocks happened before and around all large hypocenters there (Table 1). The fact that a large earthquake produces a large gap suggests that small shocks generate small crevices, which reduce the cohesion of the rock. Next, underground water percolates into the crevices. Its expansion, contraction, and chemistry further reduce the cohesion. Friction

heats the water and eventually generates vapor at high temperature and pressure. The vapor erupts from an impending hypocenter to the surface by the crevices, and rises up. It forms a cloud while encountering cold air. This kind of cloud, whose vapor is from an impending hypocenter, is denoted an earthquake cloud. Anecdotal evidence for high temperature and high pressure vapor is plentiful (2-16), as is evidence for the clouds themselves. Fig. 2 shows damage to the ceiling of a structurally intact building due to the eruption of steam from underneath it during the 7.8 Tangshan Earthquake on Jul. 28, 1976 (17).

Table 1. All big earthquakes in Southern California & their foreshocks (1981~2004)

No.	Date	Time		Lat.	Lon.	Mag. ML	Dep. km	within 5 km		within 10 km	
		UTC						All	Over	All	Over
1	19871124	1:54		33.09	-115.79	6.2	10.81	25	4	138	10
2	19871124	13:15		33.02	-115.85	6.6	11.18	186	7	558	33
3	19920423	4:50		33.96	-116.32	6.1	12.33	321	3	1602	14
4	19920628	11:57		34.20	-116.44	7.3	0.97	166	146	520	461
5	19920628	15:05		34.20	-116.83	6.3	5.38	141	128	345	256
6	19940117	12:30		34.21	-118.54	6.7	18.40	9	2	79	5
7	19991016	9:46		34.59	-116.27	7.1	0.02	250	226	430	373
8	20031222	19:15		35.71	-121.10	6.5	7.01	12	1	37	7

Note:

1. All above data are from the new catalog of the Southern California Earthquake Data Center of the USGS since 1981(@11), covering a region of 32~37N. Column 8~9 and 10~11 indicate the number of foreshocks within 5 km and 10 km of an epicenter.
2. Lat. Latitude. Lon. Longitude. Mag. Magnitude. Dep. Depth.
3. 'Over' depicts the number of foreshocks, whose depths are more than or equal to a big earthquake. For example, earthquake No. 1 has 138 foreshocks within a distance of 10 km to the epicenter, in which 10 foreshocks are deeper than or equal to 10.81 km of the M6.2 hypocenter.
4. All large earthquakes have foreshocks around their hypocenters.



7-17 丰顺县官田公社一平街内喷沙冒水，冲塌了房屋顶棚(10度区)。

In the area of intensity 10, sand boiling and water spouting occurred to a house in Yishuang Commune in Fengsan County and spoiled the ceiling.

Figure 2 Tangshan earthquake damage.

This photo shows damage in the roof of a building caused by steam erupting from the ground during the 1976 Tangshan earthquake (17). Photo ÓChina Academic Publishers.

Not only does the vapor forming the cloud originate in the Earth, but its creation is intimately linked to the subsequent earthquake. There are two important pieces of evidence. First, the USGS performed an experiment at the Rangely Oil Field in Western Colorado in 1969 (18), in which water was injected into and pumped out of oil wells. Researchers found that there was a strong positive correlation between the quantity of water injected and seismic activity. Above a threshold fluid pore pressure, seismic activity was observed to increase dramatically. Supporting this work is the results of laboratory studies of yield strength of saturated rock. As the rock is heated, the yield strength changes only gradually until a threshold temperature is reached. Past this threshold, the rock becomes dehydrated and its yield strength drops rapidly (Fig.10, (19)).

Our earthquake model is that the vapor in an earthquake cloud is precisely what escapes at the beginning of dehydration, i.e. when the yield strength begins to drop sharply. Once the yield strength has dropped sufficiently, the rock yields and an earthquake occurs. Thus, the atmospheric precursor we have discussed is directly linked to the generation of the earthquake itself.

An earthquake cloud can be distinguished from weather clouds by the following properties: a sudden appearance, a fixed source location (a fault), and a special shape such as a line, a snake, a few parallel lines, a bind of parallel waves, a feather, a radiation or a lantern pattern (2). These properties do not occur together in weather clouds (20). Fig. 3 reveals a time series of the Bam cloud that appeared suddenly from a fixed source (the Bam fault) at 2:00, Dec. 20, 2003. The dense cloud formed in the midst of light clouds and expanded eastward while remaining connected to its source. An animation will show in the OOSA web site.

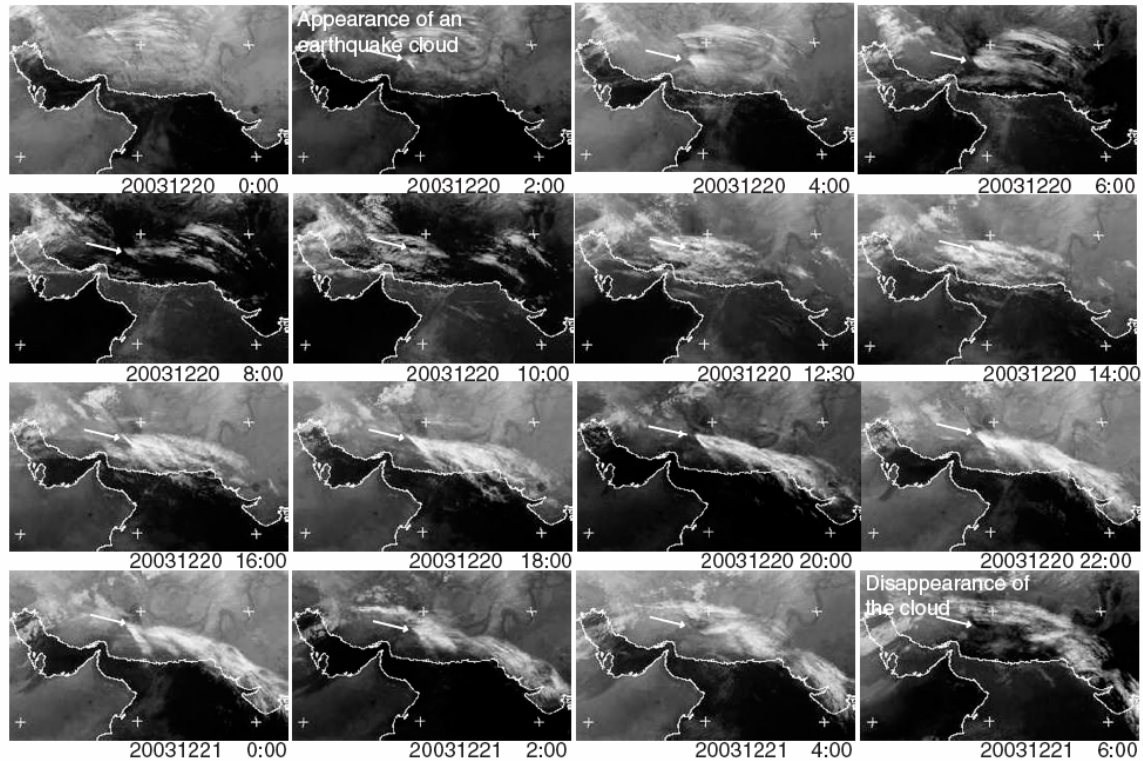


Figure 3 A Time Series of the Bam Earthquake Cloud

This series of IndoEx satellite images (@2) shows how the Bam earthquake cloud appeared suddenly, at 2:00 on Dec. 20, 2003, expanded eastward from its point of emergence, then disappeared at 6:00 on Dec. 21.

Fig. 4 depicts several examples of suddenly-appearing earthquake clouds over Southern California, including a cloud that appeared over Northridge direction 9 days before the Northridge earthquake of 1994. Fig. 5, a photo looking towards Northern California on Aug. 3, 1997 shows a cloudless line marked 4 that appeared in the midst of clouds and became a linear cloud 6 minutes after the photo was taken. Before the photo was taken, four cloudless lines had emerged rapidly, much faster than a jet trail. Two, marked 1 and 2, had entirely become line-shaped clouds and one, marked 3, had partially become a cloud for about 3 minutes. On Aug. 21, 1997 a pair of M4.9 earthquakes occurred in Northern California. The width of these features and their rapid emergence strongly support the theory that hot vapor emerges rapidly from a line-shaped region of ground (i.e. a fault).

An earthquake cloud comes from an impending hypocenter, so its tail generally points toward or predicts an impending epicenter. The more mass an earthquake cloud has, the bigger the subsequent earthquake. By comparing the mass of an earthquake cloud with those of former clouds, whose relevant magnitudes are in an earthquake catalog, the cloud can be used to predict its magnitude. Based on statistics from about 500 events, the longest delay from an earthquake cloud to its earthquake is 103 days, and their average is 30 days, so an earthquake cloud can predict the time. Therefore, an earthquake cloud can

predict an earthquake. The Bam cloud is an excellent example to show that an earthquake cloud does in fact come from the Earth.

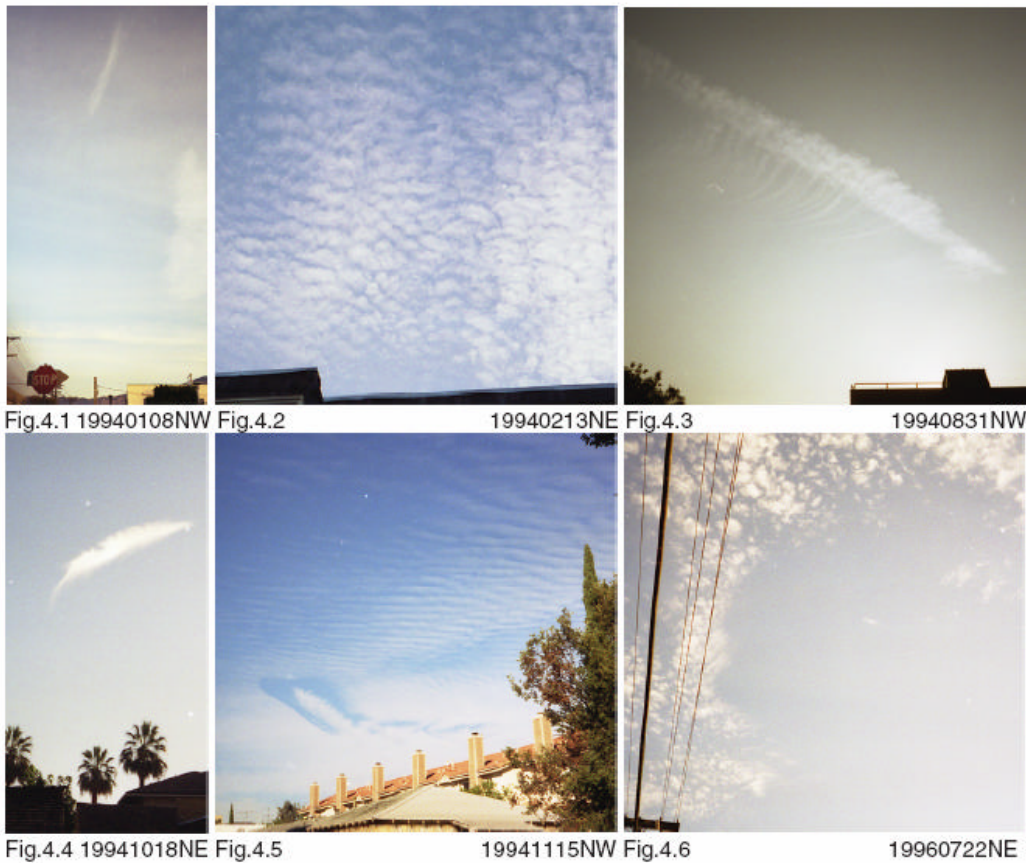


Figure 4 Various Shapes of Earthquake Clouds

Fig. 4 shows six different shapes of earthquake clouds, photographed by Shou from Pasadena (34.14 N, 118.14 W), California. Under each photo are the date and the direction Shou took the photo. The line-shaped cloud in Fig. 4.1 appeared suddenly like a launching rocket northwest of Pasadena, and predicted the 6.7 Northridge earthquake at 34.21N, 118.53W, in the same direction, on Jan. 17, 1994. The wave-shaped cloud in Fig. 4.2 was from northwest to northeast, and predicted the 5.3 Northridge earthquake on Mar. 20, 1994. The line-shaped cloud in Fig. 4.3 appeared suddenly from northwest, and predicted the 7.1 Off Coast of Northern California earthquake at 40.40N, 125.68W on Sep. 1, 1994. The feather-shaped cloud in Fig. 4.4 from northwest to northeast predicted the 6.3 Off Coast of Oregon earthquake at 43.51N, 127.42W on Oct. 27, 1994. The lantern-shaped cloud in Fig.4.5 from northwest predicted the 6.8 Off Coast of Northern California earthquake at 40.55N, 125.53W on Feb. 19, 1995. The radiation-pattern-shaped cloud in Fig. 4.6 rising up from northeast predicted the 4.4 Joshua Tree earthquake at 34.59N, 116.28W, in the same direction, on Aug. 14, 1996. All these clouds were not described by meteorology (20), but the both wave-shaped and radiation-shaped clouds were denoted earthquake clouds by Chinese and Japanese scientists in 1979 (1).



Fig. 5

19970803N

Figure 5 Northern California earthquake clouds

This photo, taken by Shou from Pasadena, California toward the north on Aug. 3, 1997, shows four lines that had appeared about 10, 8, 3, and less than 1 minute respectively, before Shou took the photo. They all emerged suddenly looking like Line 4, straight, even width, and cloudless in the midst of clouds. They each took about 6 minutes to become a white, linear cloud. In the photo, Line 1 and 2 had already become clouds, and Line 3 had partially become a cloud, while Line 4 became a cloud 6 minutes after Shou took the photo. On Aug. 21, a pair of M4.9 earthquakes occurred at 38.5N, 118.5W, to the north of Pasadena, and were the only one of magnitude more than or equal to 4 from 34N to 42N within 175 days from May 7, 1997 to Oct. 28.

Geothermal Eruption

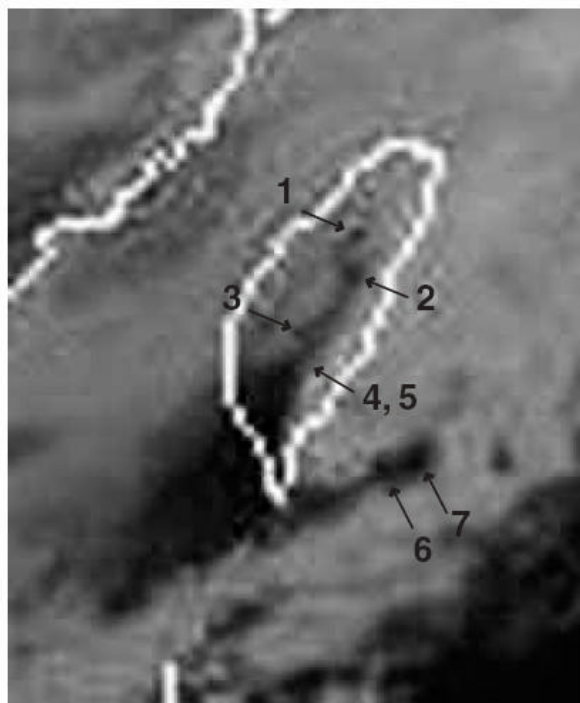
The Bam cloud was unusual since it emerged exactly from the epicenter. This was likely because its hot vapor condensed into a cloud immediately due to very cold surroundings at night during the winter. However, in many cases the vapor released at the epicenter does not immediately encounter atmospheric conditions suitable for condensation into a cloud. As a result, there is often a large distance between the first appearance of an earthquake cloud and its source. Since the cloud's travel time and direction are not well-known, this greatly reduces the precision, or specificity of the prediction.

In the search for a solution to this problem, Shou identified another atmospheric phenomenon in images from weather satellites, which we denote geothermal eruption, or

geoeruption. Geoeruption is qualitatively different from earthquake cloud although they have the same source, the impending epicenter. There are two key ingredients enabling the observer to distinguish this phenomenon in satellite weather images.

First, geoeruption emerges as a sudden localized atmospheric heating or disappearance of cloud, often occurring in the morning or evening, or covered by weather clouds or fog. In some cases the size of the emergence region is limited by the resolution of the public satellite images, about 10 km. Since the warm region often grows rapidly after its onset, to as large as 50x50 km² after one hour, variation in the size of the emergence is as likely to be an artifact of the finite frequency of the images, which varies from hourly to bidaily, as to have any physical significance. The second characteristic is the persistence of the warm region despite the presence of moving clouds overlapping or in the vicinity. Typically the warm region expands while its source point remains warm through the duration, which can be up to several days, but is normally less than one day. We believe that the emergence region of this phenomenon precisely identifies the impending epicenter.

Fig. 6 shows a snapshot of several simultaneous geoeruptions in Taiwan on Jan. 30, 2000. Over the next 46 days, one or more earthquakes of magnitude greater than 4 occurred at each of the warm regions pinpointed (Table 2).



20000130 3:00

Figure 6 Taiwan geothermal eruption

This image from the GMS satellite over Taiwan at 3:00 Jan. 30, 2000 was provided by Dundee Univ., UK (@2). Several dark spots, indicating warm regions, appear in the midst of cloud cover. Their unusual appearance leads us to believe that they were not weather-related, but instead were geothermal eruptions. Over the next 46 days, a series

of 8 earthquakes occurred at exactly the locations of the dark spots, as shown by the arrows. The earthquake data are shown in Table 2. The mottled appearance of parts of the image is a result of magnifying a small jpeg file.

Table 2 Taiwan Geoeruptions vs. Earthquakes

Geoeruptions					Earthquakes							
Date UTC	Time	P	Lat. N	Lon. E	Date UTC	Time	Lat. N	Lon. E	Mag. ML mb		Dep. Km	S
20000130	3:00	1	24.4	121.1	000131	21:11	24.37	120.9	4.6		4.2	T
					000216	19:48	24.35	120.8	4.0		7.4	T
		2	24.0	121.2	000130	20:21	23.90	121.31	4.8	4.1	33	U
							23.90	121.31	4.8		7.5	T
		3	23.5	120.7	000131	2:57	23.51	120.48	4.2		4.7	T
		4	23.2	120.7	000215	21:33	23.35	120.93		5.3	33	U
							23.33	120.75	5.6		21.1	T
		5	23.2	120.7	000216	0:33	23.33	120.75	4.5		13.4	T
		6	22.2	121.4	000226	8:23	22.24	121.37		4.1	33	U
		7	22.2	121.8	000316	0:37	22.06	121.62	5.0	4.8	33	U

Note:

1. **P:** point number. **Lat.** latitude. **Lon.** longitude. **Mag.** magnitude. **Dep.** depth. **S:** source. **U:** the USGS (@12). **T:** the Central Weather Bureau of Taiwan (@16), received by Journalist Simin Li.

2. The latitudes and longitudes of the geoeruptions were calculated directly from the image, and have an uncertainty of 0.2°.

3. The average latitude and longitude absolute errors between the earthquake and the geoeruption point of origin are 0.09° and 0.15°, respectively.

Fig. 7 shows a time series of images taken over the Eastern Mediterranean from 8:00 Feb. 23 to 2:00 Feb. 24, 2000. Based on these images, Shou made a prediction certified by the USGS on Feb. 28, 2000 that there would be an M5 or two M4 earthquakes within a coarse window of latitude 36.5N to 38.5N, longitude 36E to 39E (shown in the figure) and 50 days from Feb. 28 to Apr. 18, and a fine window of latitude 37N to 37.8N, longitude 36.8E to 37.2E (too small to show) and 17 days from Mar. 25 to Apr. 10. The prediction was correct, as two earthquakes occurred at point B, well within the coarse window, at the edge of the fine window, and coinciding with a bulge in the geoeruption. No other earthquakes of magnitude bigger than or equal to 4 have occurred in the fine area window in more than 14 years since the beginning of the database on Jan.1, 1990. Within the fine time window, the predicted pair were the only earthquakes bigger than or equal to 4 in the region 29~44N, 31~48E, a region 637 times larger than the predicted area. Earthquakes also occurred later at points A and C, again coinciding with geoeruption features (Table 3).

Similar to an earthquake cloud, a geoeruption can predict an earthquake for three reasons. First, its tail points toward the epicenter. Second, its mass indicates the magnitude. Third, its longest observed delay is 104 days, and the average is about 30 days.

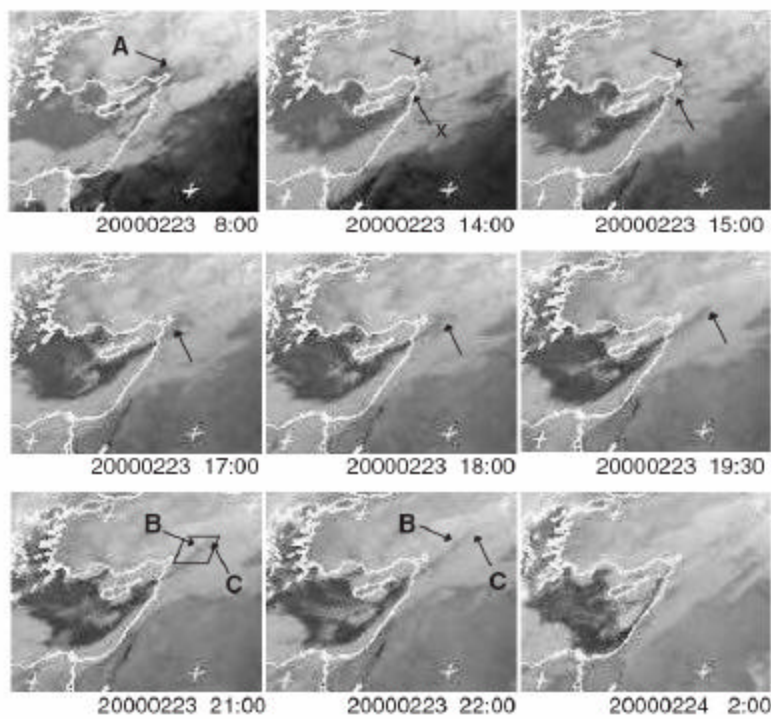


Figure 7 Turkey geothermal eruptions

This series of IndoEx satellite images of the Eastern Mediterranean was provided by Dundee Univ. (@2). A georruption had occurred in Turkey at Point A (37N, 36.1E) at 8:00 Feb. 23, 2000, and disappeared at 15:00. Meanwhile, another warm spot appeared at Point X and grew toward the northeast. Two small bulges appeared at Points B (37.8N, 37.2E) and C (38.2N, 38E) at 21:00. Based on the feature at Point B. Shou predicted an earthquake to the USGS. The coarse area window of the prediction is shown by the black rectangle and the fine area window coincides with Point B. Two earthquakes of magnitude 4.2 and 4.4 occurred at Point B on Apr. 2, 2000, 39 days later. Earthquakes also occurred at A on May 12 and C on May 7. All data are shown in Table 3.

Table 3 Turkey Geoeruptions vs. Earthquakes

Geoeruptions					Earthquakes					
Date UTC	Time	P	Lat. N	Lon. E	Date UTC	Time	Lat. N	Lon. E	Mag. mb	Dep. Km
20000223	8:00	A	37.0	36.1	000512	3:01	37.05	36.08	4.7	10
	21:00	B	37.8	37.2	000402	11:41	37.57	37.19	4.2	9
					000402	17:26	37.65	37.23	4.4	9
	22:00	C	38.2	38.0	000507	9:08	38.18	38.75	4.2	1.6
					000507	23:10	38.16	38.78	4.5	5.4

Note:

P. Point of a georruption in Fig. 7. Lat. Latitude. Lon. Longitude. Mag. Magnitude. Dep. Depth. The earthquake data are from the USGS (@12), and the average latitude and longitude absolute errors between the earthquake data and the georruption data are 0.10° and 0.32°, respectively.

Statistical Significance

To objectively evaluate the significance of an earthquake prediction, Shou proposed a probability calculation to simulate a random time guess. From a comprehensive earthquake database, select all earthquakes whose epicenters are within the predicted area and whose sizes are within the predicted magnitude range. Consider all time windows of the same time span as the prediction, using 1-day resolution. If a time window guess contains one or more of those selected earthquakes, it is a hit. Let A be the number of all hits, and B be the number of all time windows, then the probability for a random guess with the same time span to be correct is A/B (2). Table 4 selects all earthquakes of magnitude more than or equal to 5 in Fault AB from the World Earthquake Catalog of the USGS (@12) from Jan. 1, 1990 to Dec. 20, 2003, together 5102 days. The coarse time span of Shou's Bam prediction is 98 days, so $B = 5102 - 98 + 1 = 5005$. The table reveals $A = 98$, so the probability is $A/B = 1.96\%$ for the coarse prediction. For the fine prediction, there was no earthquake in the database, so its probability is close to 0. Therefore, the Bam earthquake prediction shows that earthquakes can be predicted in practice.

Table 4 the probability of the Bam earthquake prediction

	Latitude(N)	Longitude(E)	Magnitude	Coarse hits	Fine hits
19900101					
19980610	28.27	58.54	5.4	98	0
20031220					
Sum				98	0
Probability				98/5005	0/5043

Note: The period from Jan. 1, 1990 to Dec. 20, 2003 contains 5102 days. For the coarse prediction, it has $5102 - 98 + 1 = 5005$ different time windows, whose spans are as the same as the predicted span, 98 days, such as (19900101~19900408), (19900102~19900409), etc. The database lists only one M5.4 earthquake in the coarse prediction area window. Together 98 time windows, those beginning from Mar. 5, 1998 to Jun. 10, include the M5.4, so $A = 98$ and its probability is $98/5005$, or 1.96%. The database lists no earthquakes of magnitude 5.5 or greater in the fine prediction area window. Out of 5043 time windows of length 60 days, there are no hits, so the fine prediction probability is negligibly small (less than $\sim 1/5000$).

Based on observations of earthquake clouds and geoeruptions, both visible and infrared satellite images, Shou submitted 50 earthquake predictions between 1994 and 2001 to be certified by the USGS. Table 5 exhibits all of them, and their subsequent earthquakes, as reported in USGS databases. Assuming all earthquake data is without error, so called "Peer on", 34 predictions or 68% of them are correct in time, location, and magnitude. They are called "hits", while the others "misses".

To evaluate the statistics, we adopt an unpublished method by Jones (@13) and Jones (@14) to evaluate a set of independent predictions. If a prediction has a probability p , it is assigned a positive score $-\ln p$ when it is a hit, or a negative score $\ln(1-p)$ when a miss (21). For a set of predictions, the normalized score S is the total score (sum of the individual scores) divided by the standard deviation of the total score. The distribution of S can be approximated as a normal distribution and thus the probability for a random guesser to equal or exceed the score is evaluated from the normal distribution (22) or (@15). For Shou's 50 certified predictions, the total score is 3.84, giving a chance of only 0.00062, or

1 in 16,000 for a random guesser. We also performed a direct computer simulation of the random guesser, which gave a chance of 0.00018, or 1 in 5,000 to achieve 34 or more correct predictions out of 50, given the calculated probabilities for individual predictions. This clear statistical significance validates the prediction method.

Table 5. Shou's 50 Earthquake Predictions reported to the USGS

No.	P r e d i c t i o n s				E a r t h q u a k e s					Prob. (%)	Hit	Score	Var.
	Date	Time (LT)	Location	M	Date	Time	Lat.	Lon.	M				
1	940213	0213-0310	Around Pas.	4-5.5	225	12:59	34.36	-118.48	4.1	13.8	1	1.84	0.54
2	940330	0330-0424	Cal.	5-7	406	19:01	34.19	-117.1	5	27.1	1	1.18	0.52
3	940423	0423-0518	N Mex., S Cal.	>=4	512	00:22	25.07	-109.28	5.6	73.1	1	0.44	0.52
4	940603	0603-0628	S Cal.	3.7-5.5	615	05:59	34.31	-118.4	4.2	79.6	1	0.37	0.54
5	940910	0910-0925	20-50, 0-75	>=6	1025	00:54	36.36	70.96	6.2	20	0	-0.37	0.54
6	940916	0916-1011	Japan ~ Ale. < 500km	>=5	1004	13:22	43.77	147.32	8.3	99.9	1	0.01	0.05
7	941018	1018-1112	USA	>=5	1027	17:45	43.52	-127.43	6.3	48.1	1	0.72	0.48
8	950307	0307-0401	Mex., S Cal.	>=4	326	14:32	31.26	-114.35	4.2	100	1	0	0
9	950630	0630-0720	S Cal.	>=5	630	11:58	24.69	-110.23	6.2	8.9	0	-0.22	0.51
10	951011	1011-1105	Cal.	>=5	1021	02:39	16.84	-93.47	7.2	27.1	0	-0.44	0.52
11	960510	0510-0530	S Cal.	3.7-5.3	521	20:50	37.36	-121.72	4.8	31.6	0	-0.48	0.51
12	961025	1025-1119	S Cal.	>=4.5	1127	20:17	36.08	-117.65	5.3	28.5	0	-0.45	0.52
13	961125	1125-1220	Mex. ~ Peru	>=6	1231	12:41	15.83	-92.97	6.4	44.8	0	-0.63	0.48
14	961204	1204-1229	S Cal., N Mex. >30N	4-5.3	1217	04:03	36.08	-117.65	4	48	1	0.72	0.48
15	961206	1206-0105	Mex.	>=4.5	1208	23:52	14.99	-94.02	5	98.1	1	0.08	0.3
16	970306	0306-0405	N China >35N	>=6	405	23:46	39.51	76.87	5.9				
		0405 20:36			406	04:36	39.54	77	6	12.8	1	1.91	0.54
17	970424	0424-0610	S Cal.	>=4	426	10:37	34.37	-118.67	5.1	79.4	1	0.37	0.54
					427	11:09	34.38	-118.65	4.9				
18	970427	0427-0611	S Cal.	3.7-5.3	506	19:12	35.45	-118.43	4.5	93.7	1	0.18	0.47
19	970508	0508-0608	S Cal.	4-5.3	524	04:36	35.8	-117.64	4	63.4	1	0.53	0.5
20	970528	0528-0712	Turkey & Med. >=15E	>=5.5	630	21:48	36.63	31.41	4.5	35.6	0	-0.52	0.5
21	970718	0719-0809	S Cal.	>=4	726	03:14	33.4	-116.35	4.8	50.2	1	0.69	0.48
22	970804	0804-0828	S Cal.	>=4	821	16:11	38.57	-118.5	4.9	34.1	0	-0.51	0.5
						16:36	38.56	-118.49	4.8				
23	980105	0105-0218	25-41, 53-105	>=6	204	14:33	37.07	70.09	6.1	44.1	1	0.78	0.48
24	980106	0106-0220	Mex.	>=5	203	03:02	15.88	-96.3	6.4	79.5	1	0.37	0.54
25	980309	0309-0423	15-30, <150	>=4	507	23:15	19.22	-155.51	4.3	31.7	0	-0.49	0.51
26	980406	0406-0522	Mex., Cal., <34N	>=4.5	425	11:19	17.68	-94.19	5.2	99.3	1	0.03	0.17
27	980724	0724-0902	34-39, -119--117	4-5.5	801	06:01	37.58	-118.78	4.4	54.9	1	0.63	0.48
28	981123	1123-0109	Cal. <39N	>=4.5	1212	01:41	37.51	-116.29	4.5	72.3	1	0.45	0.52
29	981228	1228-0213	33-39, -120--116	4.2-5.4	125	18:52	36.81	-116.04	4.2	69.9	1	0.47	0.51
30	990222	0222-0408	20-38, 50-100	>=5.5	304	05:38	28.34	57.19	6.6	61.8	1	0.55	0.49
31	990402	0402-0520	24-34, -118--108	4-5.2	428	19:08	30.3	-115.54	4.5	77.6	1	0.39	0.53
						19:34	30.25	-115.61	4.4				
32	990412	0412-0529	34-39, <116	>=4	514	07:54	34.06	-116.37	4.9	83.1	1	0.33	0.54
33	990505	0505-0621	27-33, -117--113	>=4	601	15:18	32.37	-115.24	5.1	40	1	0.86	0.49
34	990517	0517-0704	Mex. <29N	>=5	615	20:42	18.39	-97.44	7	79.5	1	0.37	0.54
35	990609	0609-0725	35-39, -120--116	4-5.3	711	18:20	35.73	-118.48	4.6	61.9	1	0.55	0.49
36	990726	0726-0910	36-42, 113-117	>=5	817	10:41	29.41	105.61	4.8	4.7	0	-0.15	0.43
37	991028	1028-1214	30-33, -117--115	>=4.3	1114	14:20	34.84	-116.41	4.5	15.7	0	-0.32	0.54
38	991227	1227-0210	Indian Ocean >20S	>=7	209	18:40	-27.62	65.72	5	0	0	0	0
					209	18:40	-27.69	65.71	5				
					210	14:18	-27.58	65.73	5.7				
					210	14:18	-27.66	65.68	5.7				
					210	23:00	-27.58	65.78	5.5				
					210	23:00	-27.63	65.76	5.6				
39	000228	0228-0413	31-35, -116.5--115	>=4.5	409	10:48	32.69	-115.39	4.3	21.6	0	-0.38	0.53
40	000705	0705-0821	Japan <34, <142.5	>=6	730	12:25	33.9	139.38	6.5	32.2	1	1.03	0.51
41	010321	0321-0505	Cal. >38N	>=4	322	21:22	40.48	-126.18	4.7	80	1	0.37	0.54
42	010806	0806-1021	21-25, 68-73	>=6	920	13:24	23.57	70.28	4.7	0	0	0	0
					921	02:40	23.47	70.07	4.5				
43	010808	0808-1002	32-33.5, -117--115.2	>=4	1031	07:56	33.51	-116.51	5.2	8.4	0	-0.22	0.51

44	990825	0825-1003	N Cal. >38,<-122	>=5.5	818	1:06	37.91	-122.69	5	6	0	-0.17	0.47
45	000228	0228-0418	36.5-38.5,36-39	1M5/2M4	402	11:41	37.57	37.19	4.2	6.8	1	2.57	0.48
						17:26	37.65	37.23	4.4				
46	000322	0322-0505	35.8-40,-120--117	>=4	328	15:16	36.02	-117.87	4.3	37.7	1	0.9	0.49
47	000629	0629-0820	Japan, <37	>=6	701	07:01	34.22	139.13	6.2	37.7	1	0.9	0.49
48	010320	0320-0504	N Cal., -126--122	>=4.5	420	05:19	40.68	-125.32	4.8	29.3	1	1.11	0.51
49	010426	0426-0615	USA-Can,38-54,<-120	1M5/2M4	502	02:05	49.91	-130.15	5.3	71.7	1	0.45	0.52
50	010403	0403-0702	36.3-37.2, -121.5--120	>=4	702	17:33	36.7	-121.33	4.1	18.8	1	1.53	0.54
Sum											34	18.34	
S.Dev													4.78
Total Score												3.84	

Note:

1. Shou's 50 predictions were reported to the USGS from 1994 to 2001. All of the m are independent, e.g. No.17 and No.18 seem dependent, but No. 18 was made after No. 17 had hit an earthquake. Similar, No. 18 and No. 19, and No. 28 and No. 29 are independent, too. Shou's predictions have coarse and fine windows. Here are all coarse. No. 1~43 and No. 44~50 predictions rely on the clouds and geoeruptions respectively.
2. In Column3, LT is Los Angles Time, while in Column 6 and 7, Time is UTC. The M6.0 earthquake for No. 16 prediction happened at 4:36 on Apr. 6 UTC or at 20:36 on Apr. 5 LT, mentioned in Column 3, so the prediction is correct.
3. In Column 4, Ale. Aleutian. Cal. California. Can. Canada. Med. Mediterranean. Mex. Mexico. Pas. Pasadena (34.138 N, 118.143 W).
4. All earthquake data are from the USGS (@12) except No. 29 from both the Northern California Earthquake Data Center of the USGS (@17) and Univ. of Nevada (@18).
5. In Column 5, M. Magnitude. 1M5/2M4 means one earthquake of magnitude 5~5.9 or two 4~4.9. In Column 10, we adopt the maximum magnitude if there are few recordings, as is customary.
6. In Column 8 and 9, Lat. Latitude. Lon. Longitude.
7. In Column 11, Prob. probability according to Shou's calculation (2).
8. In Column 12, '1' means the prediction is correct in time, location, and magnitude, checked with "Peer on" i.e. assuming earthquake data is without error; while '0' means incorrect. Together, 34 predictions or 68% of them are correct.
9. In Column 13, Score adopts Brelsford & Jones' method (21). If a prediction has a probability **p** correctly, it will have a positive score $-\ln \mathbf{p}$, while a negative score $\ln (1-\mathbf{p})$ when it is incorrect. The total score is the sum of individual scores, or 18.34.
10. In Column 14, Var.: variance = $\mathbf{p} (1-\mathbf{p}) [\ln \mathbf{p} (1-\mathbf{p})]^2$. The standard deviation of Shou's total score is 4.78.
11. The normalized score is the total score divided by the standard deviation of the total score (Jones (@13) - Jones (@14)). The normalized score for Shou's set is 3.84. Comparing it with the normal distribution (@15) or (22), the total probability of Shou's set is 0.000062.

Analysis of Errors

Let's look at the 16 misses. The prediction of Aug. 25, 1999 was the result of a clerical error, Shou having submitted the prediction after the earthquake had already occurred. Five misses were due entirely to time window errors, in general the choice of too small a window. Such errors were a natural consequence of the process for developing an empirical method, as the time delay between precursor and earthquake is not known theoretically. Six misses were due entirely to area errors, because the earthquake clouds often appeared far from epicenters, and satellite data did not clearly reveal their origin

The other 4 misses were in magnitude. Two were due to a phenomenon in which the observed atmospheric feature came from two or more closely spaced impending epicenters. For example, Shou predicted an earthquake of magnitude more than or equal to 7 in the Indian Ocean with a latitude over 20S from Dec. 27, 1999 to Feb. 10, 2000, and likely in the area of latitude 25~28S, and longitude 60~80E by the cloud of Fig. 8. However, not one M7, but 6 M5 earthquakes occurred in the time and the fine area instead (Table 5). The six earthquakes are the only sextuplets of magnitude more than or equal to 5 in the entire Indian Ocean within 3,000 days from May 27, 1994 to Aug. 12, 2002. Similarly, prediction number 42 gives a couple of twins.

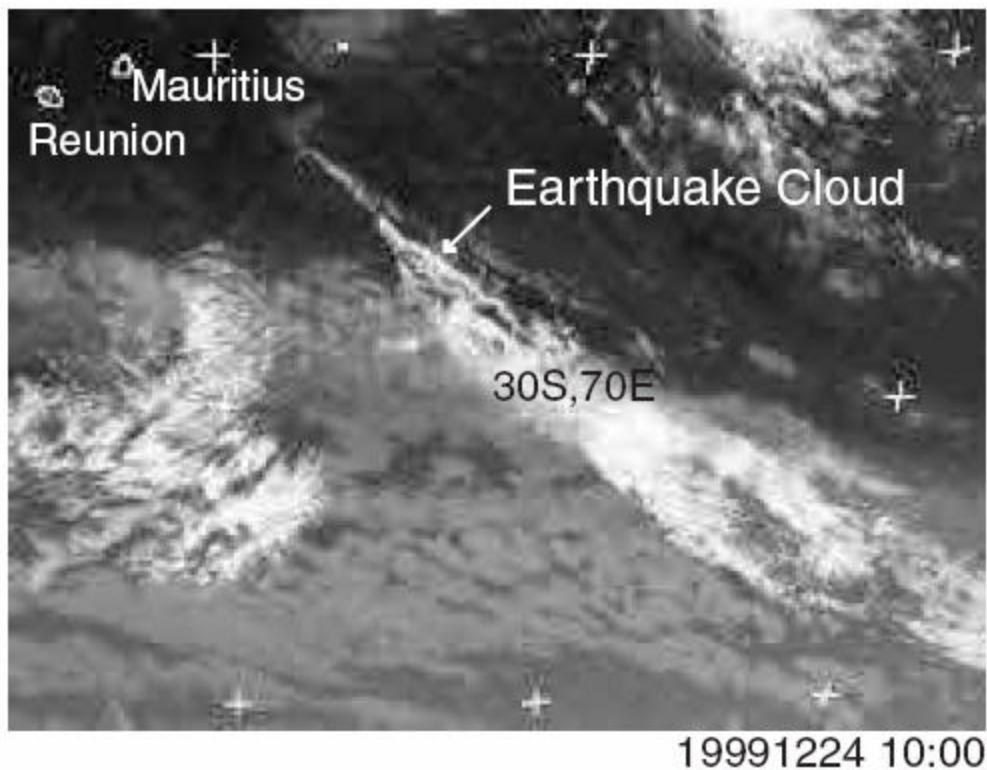


Figure 8 the Union of Six Earthquake Clouds

This Infrared image of IndoEx satellite (©2) revealed a linear cloud, marked by arrow near 30S, 70E over the Indian Ocean at 10:00, Dec. 24, 1999. By this cloud, 550 km in length, Shou predicted an M7 earthquake over 20S in the Indian Ocean from Dec. 27, 1999 to Feb. 10, 2000, with a fine area window of 25~28S and 60~80E. However, not one M7, but 6 M5 earthquakes occurred in this window on Feb. 9~10, 2000 (Prediction No. 38 in Table 5).

Another difficulty is the uncertainty in even the highest quality earthquake data. For example, the USGS changed the magnitude of 5.8Mb in Rank “A” to 5.3Mb in Rank “A” for the Iran -Turkmenistan border earthquake on Nov. 19, 1999. It implies error in Rank “A” reaching 0.5Mb, which is much higher than the 0.1Mb uncertainty quoted by seismologists. This is a significant problem both for the evaluation of earthquake predictions and the development of the empirical method.

The above analysis reveals that the few incorrect predictions do not cast doubt on the validity of the precursors, but instead suggest that more attention must be paid to data quality and data interpretation.

Impact of Space Technology

Clearly, the use of space technology has been essential to the development of an earthquake prediction method based on atmospheric precursors. Satellite imagery is by far the most practical way to obtain global round-the-clock coverage. A good example is the magnitude 6.1 Afghanistan quake of Feb. 4, 1998. The portion of a global composite shown in Fig. 9 reveals the distinctive cloud that was used to make a successful prediction to the USGS.

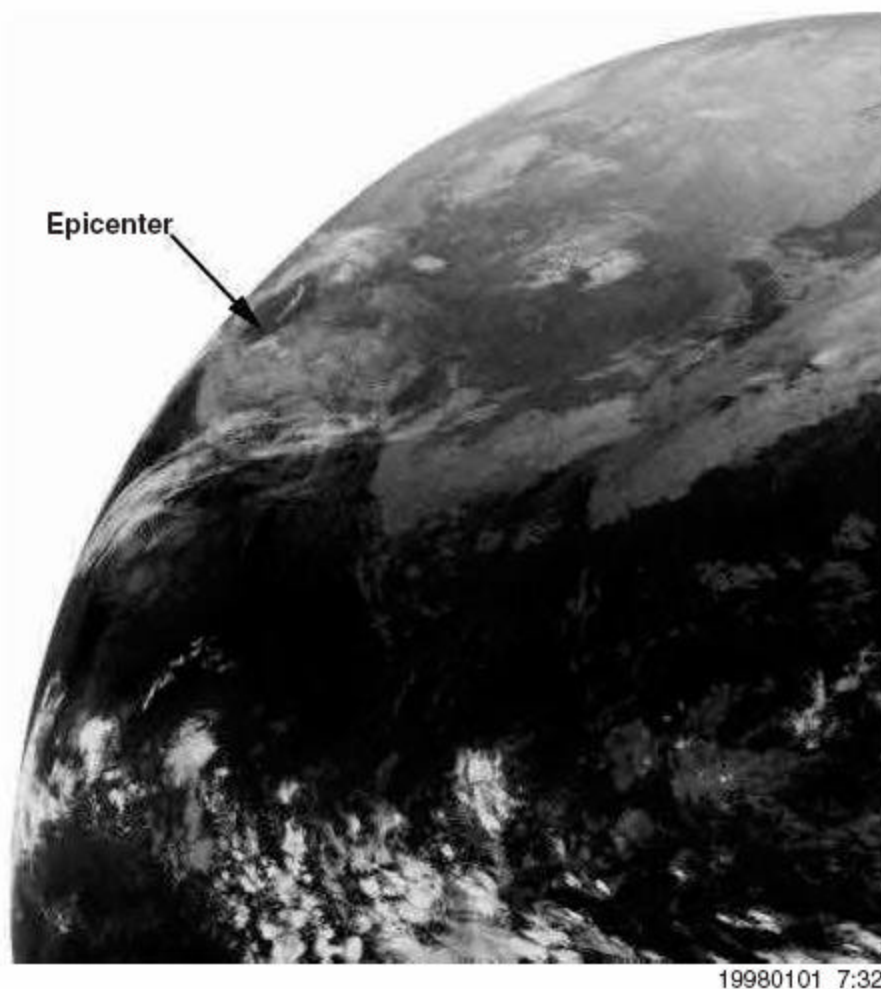


Figure 9 the M6.1 Afghanistan earthquake cloud

This image was taken from a composite of the GMS satellite, provided by University College London (@3). At about 7:32 Jan.1, 1998, a hole with a line-shaped cloud inside appeared in a large weather cloud. The line-shaped cloud disappeared at about 16:25. Shou predicted an earthquake of magnitude larger than or equal to 6 in Afghanistan and its neighbors, with a coarse window of 25~41N and 53~105E from Jan. 5 to Feb. 18, and a fine window of 30~37N and 58~95E, from Jan.5 to Feb.4, 1998 to the USGS. The 6.1 Afghanistan earthquake at Rustaq (36.83~ 37.31N, 69.5~70.11E) (@19) marked by the tip of the arrow, on Feb. 4 proved the both coarse and fine predictions correct.

Using satellite images of atmospheric precursors, Shou has successfully predicted 50 earthquakes, including a pair of 6.0 Xinjiang, China earthquakes on Apr. 5 and 6, 1997, the 6.4 Mexico Feb. 3, 1998, the 6.1 Afghanistan Feb. 4, 1998, the 6.6 S Iran Mar. 4, 1999, the 7.0 Mexico on Jun. 15, 1999, the 6.2 Japan Jul. 1, 2000, and the 6.5 Japan Jul. 30, 2000 to the USGS. He has also predicted the 7.0 Mexico earthquake on Jun. 15, 1999, the 7.4 Hector Mine, S California Oct. 16, 1999, the 6.2 Japan Jul. 1, 2000, the 6.5 Japan Jul. 30, 2000, the 6.8 Seattle Feb. 28, 2001, the 6.5 W Iran Jun. 22, 2002, the 7.6 Mexico Jan. 22, 2003, the 6.4 Gulf of California Mar. 12, 2003, the 7.0 Japan May 26, 2003, the 6.8 Chile on Jun. 20, 2003, the 6.0 Yunnan, China Jul. 21, 2003, the 6.8 Bam, Iran Dec. 26, 2003, the couple of 5.5 Pakistan Feb. 14, 2004, among others, to the public (@1).

However, the scope of our work currently suffers from four important limitations. First, an earthquake cloud appearing in satellite images can pinpoint an impending epicenter from an earthquake cloud only when it condenses at the epicenter in cold surroundings, as it did in Bam. As a result, the area windows must often be made very large, thus reducing the usefulness of the prediction. For example, Shou had known of an impending earthquake of magnitude over 7 from Iran to Italy within 49 days following Jul. 16, 1999 relying on a long, linear cloud imaged near Sri Lanka (Fig. 10). However, he did not know the exact epicenter until the 7.8 Turkey earthquake on Aug. 17, 1999 because the images did not show from the cloud's origin.

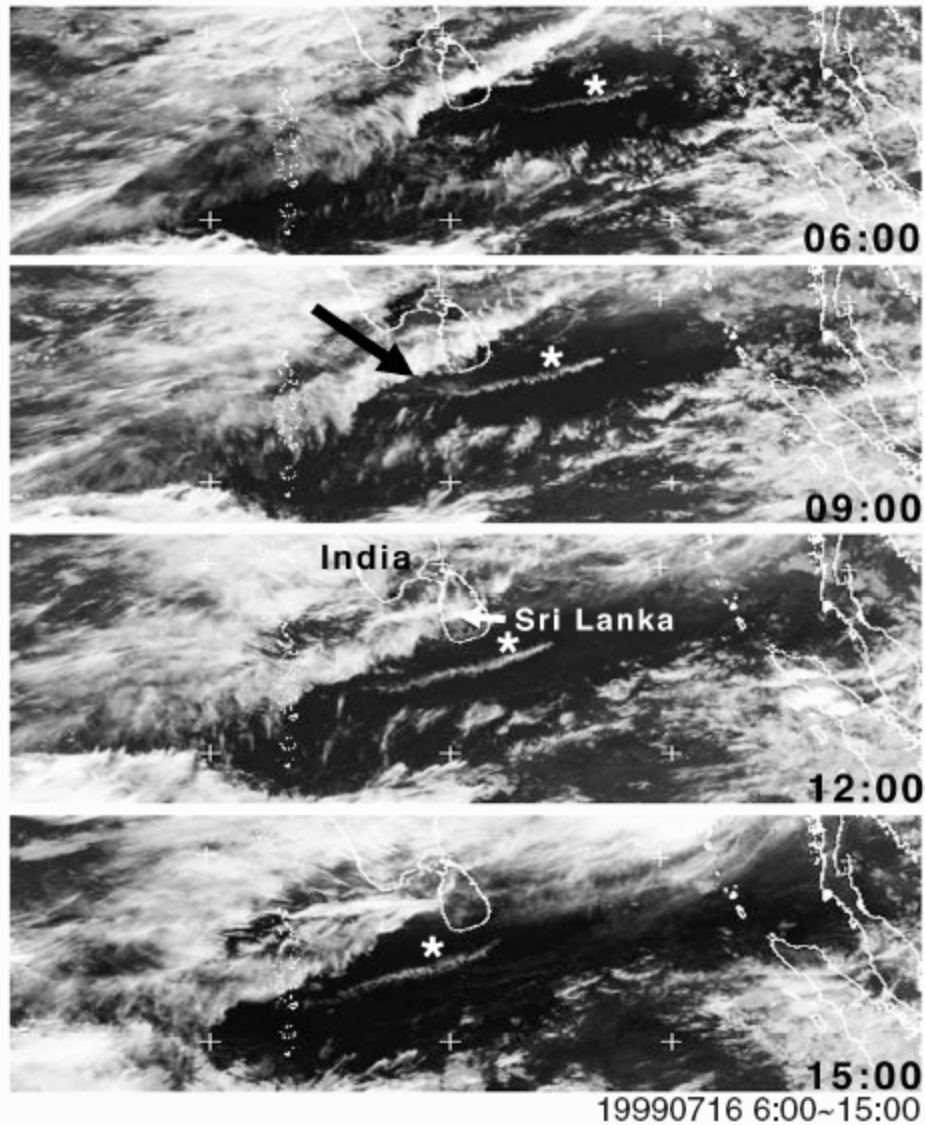


Figure 10 the 7.8 Turkey earthquake cloud

These infrared images were from the IndoEx satellite (@2) from 6:00 to 15:00 on Jul.16, 1999. At 6:00, a linear cloud appeared in a large clear sky near Sri Lanka. The cloud lengthened as it moved eastward, and then disappeared after 15:00. The length of the cloud, 800 km, suggested an earthquake of magnitude over 7. The tail (see 9:00) pointed to the northwest, and indicated that the epicenter would be in a region from Iran to Italy. However, the satellite images did not show the exact epicenter, and Shou did not know it until Aug. 17, 1999 when the 7.8 Turkey earthquake happened at 40.74N, 29.86E.

Fig. 11 shows a comparison between simultaneous visible and infrared images of California at 15:30 of Mar. 20, 2001. The visible image clearly shows a dark trace of a georruption from Hollister, California, by which Shou predicted an earthquake of magnitude more than or equal to 4 there, circled at the beginning of the trace, from Apr. 3 to Jul. 2, 2001 to the USGS and the public. On Jul. 2, an M4.1 earthquake happened there (36.7N, 121.3W) exactly. In contrast, the infrared image did not reveal the georruption. This comparison highlights the importance of selecting an appropriate imaging band and the target of the image post-processing to expose the origin of earthquake vapor. The existence of georruption phenomena suggests that if we could solve this problem, we may

be able to pinpoint all large epicenters in satellite images, independent of their surrounding environment.

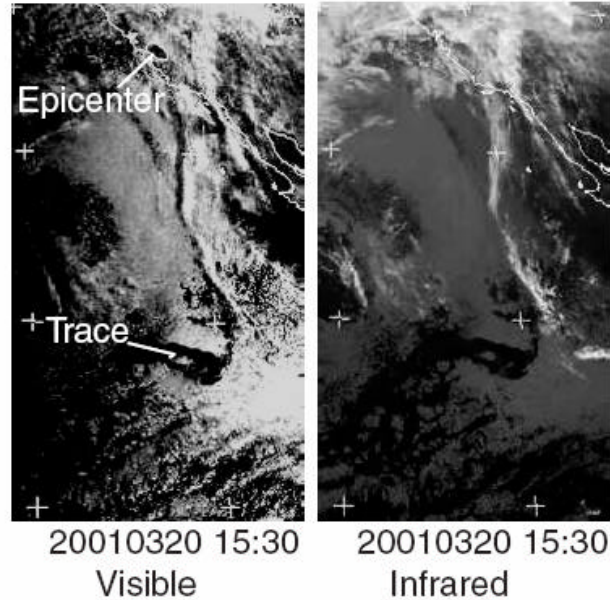


Fig. 11 A Comparison between Visible & Infrared

Two simultaneous images, visible and infrared were taken by Goes-West (@2) of the same location at 15:30 on Mar. 20, 2001. The visible image clearly showed the black trace of a geoeruption from Hollister, California to the ocean, while the infrared did not. Shou used this geoeruption to successfully make prediction No. 50 in Table 5.

Second, many earthquake clouds and geoeruptions are likely missed due to their short lifetimes and sudden appearance. For example, the Northridge earthquake cloud existed for only 35 minutes according to Shou's visual record, and typical lifetimes range from half hour to 10 hours. The frequency of public satellite images for some locations ranges from ½ hour to 6 hours, depending on location, and even in high frequency regions individual images are often unavailable. The Bam cloud in Fig. 2 appeared at 2:00 on Dec. 20, 2003, while nothing was seen in the previous image at 0:00. Increasing the image frequency would not only increase the likelihood of identifying an atmospheric precursor, but would also help to improve the reliability of predictions by clearly revealing the growth of the cloud or geoeruption from a fixed source. This may be more of a satellite data management issue than a technical problem.

Third, public weather satellite images do not have high enough resolution to resolve closely spaced atmospheric precursors, such as those shown in Fig. 7 and 8. As a result, multiple small earthquakes can be mistaken for a single large earthquake, as described in the Error Analysis section. On the other hand, the Advanced Very High Resolution Radiometer (AVHRR) can give 1.1-km resolution, much better than the 4 km of images for the public. The authors have not yet had the opportunity to study those data, but expect that they will provide the necessary detail.

Finally, the amount of time needed to search satellite images by eye for atmospheric precursors severely limits the number of earthquake predictions that can be made by a



single individual. To apply this prediction method to a large fraction of the world's earthquakes will require the development of satellite imagers and automatic image processing techniques that are tailored to find the hot vapor emerging at an impending epicenter. It is quite possible that both the imagers and the techniques already exist, and need only be redirected to this target.

With a moderate amount of international effort devoted to solving the problems of imaging, data processing and management, this method of earthquake prediction by atmospheric precursors could finally provide governments and communities around the world with information that was once thought unknowable: the time, place and size of every significant impending earthquake.

Acknowledgement

The authors gratefully acknowledge Wenying Shou and Frank Mayhar for support, UN Space Applications Section Office for Outer Space Affairs, Alice Lee, Sharafat Gadimova, UN/Islamic Republic of Iran Regional Workshop, Iran Space Agency, Hassan Shafti, Parviz Tarikhi, and Abdolreza Ansari Amoli for the invitation, Dundee University, UK and University College London for satellite images, Orhan Cerit for the animation, the United States Geological Survey, UN Office for the Coordination of Humanitarian Affairs, the Southern and the Northern California Earthquake Data Centers, University of Nevada, the Central Weather Bureau of Taiwan, and Simin Li for earthquake data, China Academy of Building Research and China Academic Publishers for the photograph of earthquake damage, and Alan L. Jones and Richard H. Jones for methods of statistical evaluation.

References

1. Li, D.J. Earthquake Clouds, 148-150 (Xue Lin Public Store, Shanghai, China, 1982) in Chinese.
2. Shou, Z.H. Earthquake Clouds a reliable precursor. *Science & Utopia* **64**, 53~57 (1999) in Turkish.
3. Haicheng Earthquake Study Delegation. Prediction of the Haicheng earthquake. *Eos* **58**, 236-272 (1977).
4. Spray, J.G. A physical basis for the frictional melting of some rock- forming minerals. *Tectonophysics* **204**, 205-221 (1992).
5. Swanson, M.T. Fault structure, wear mechanisms and rupture processes in pseudotachylyte generation. *Tectonophysics* **204**, 223-242 (1992).
6. Koch, N. & Masch, L. Formation of Alpine mylonites and pseudotachylytes at the base of the Silvretta nappe, Eastern Alps. *Tectonophysics* **204**, 289-306 (1992).
7. Techmer, K.S., Ahrendt, H. & Weber, K. The development of pseudotachylyte in the Ivrea-Verbano zone of the Italian Alps. *Tectonophysics* **204**, 307-322 (1992).
8. Shi, H. X., Cai, Z.H. & Gao, M.X. Anomalous migration of shallow groundwater and gases in the Beijing region and the 1976 Tangshan earthquake. *Acta Seismologica Sinica* **2**, No.1, 55-64 (1980) in Chinese.
9. Yang, C.S. Temporal and spatial distribution of anomalous ground water changes before the 1975 Haicheng earthquake. *Acta Seismologica Sinica* **4**, No.1, 84-89 (1982) in Chinese.
10. Glowacka, E. & Nava, F. A. Major earthquakes in Mexicali Valley, Mexico, and fluid

extraction at Cerro Prieto geothermal field. *Bulletin of the Seismological Society of America* **86, No.1A** , 93-105 (1996).

11. Haas, J.L.Jr. The effect of salinity on the maximum thermal gradient of a hydrothermal system at hydrostatic pressure. *Eco. Geol.* **66**, 940-946 (1971).

12. Chandrasekharam, D. Ateam emanation due to seismic pumping, Killari, Maharashtra. *Geol. Surv. Ind. Spl. Pub.* **No.27**, 229-233 (1995).

13. Lane, T. & Waag, C. Ground-water eruptions in the Chilly Buttes area, Central Idaho. *Special Publications* **91**, 19 (1985).

14. Shi, H.X. & Cai, Z.H. Case examples of peculiar phenomena of subsurface fluid behavior observed in China preceding earthquakes. *Acta Seismologica Sinica* **2, No.4**, 425-429 (1980) in Chinese.

15. Zhang, D.Y. & Zhao, G.M. Anomalous variations in oil wells distributed in the Bohai bay oil field before and after the Tangshan earthquake of 1976. *Acta Seismologica Sinica* **5, No.3**, 360-369 (1983) in Chinese.

16. Tang, X. Anomalous meteorology. *A General History of Earthquake Study in China*, 49-84 (Science Press, Beijing, 1988) in English.

17. China Academy of Building Research. *The Mammoth Tangshan Earthquake of 1976 Building Damage Photo Album*. 167 (China Academic Publishers. Beijing, 1986) in both Chinese and English.

18. Bolt, B.A. Stimulation of earthquakes by water. *Earthquakes*, 135-139 (W.H. Freeman and Company, New York, 1988).

19. Kirby, S.H & McCormick, J.W. Inelastic properties of rocks and minerals: strength and rheology. *Practical Handbook of Physical Properties of Rocks and Minerals*, 179- 185 (ed. Carmichael, R.S., CRC Press, Boca Raton, Florida, 1990).

20. Ahrens, C.D. *Meteorology Today*. (West Publishing Company, St. Paul, MN, 1991).

21. Brelford, W.M. & Jones, R.H. Estimating Probabilities. *Monthly Weather Review* **95**, 570-576 (1967).

22. Sir Ronald A. Fisher *Statistical Methods for Research Workers* 77 (T. and A. Constable Ltd., Edinburgh, Great Britain, 1970).

Web Sites

@1 Earthquake Clouds & Short Term Prediction

<http://quake.exit.com>

@2 DSRS Geostationary Satellite Imagery of Dundee Univ., UK

<http://www.sat.dundee.ac.uk/pdus.html>

@3 University College London

<ftp://weather.cs.ucl.ac.uk/Weather/>

@4 NOAA Satellite & Information Services

<http://noaasis.noaa.gov/NOAASIS/>

@5 OSU Weather of Ohio State Univ.

<http://asp1.sbs.ohio-state.edu/>

@6 EUMETSAT, German

<http://www.eumetsat.de/en/index.html>

@7 Satellite Imagery of Utah Univ.

<http://www.met.utah.edu/jhorel/html/wx/satellite.html>

@8 Space Science & Engineering Center of Univ. of Wisconsin-Madison

<http://www.ssec.wisc.edu/>

@9 Meteosat images of the Univ. of Nottingham, UK

<http://www.nottingham.ac.uk/meteosat/>

@10 Earth & Space Science of Univ. of Washington

<http://www.geophys.washington.edu/>

@11 Catalog of the Southern California Earthquake Data Center

<http://www.data.scec.org:3128/ftp/catalogs/SCSN/>

@12 Ftp Catalog of the US Geological Survey (USGS)

http://wwwneic.cr.usgs.gov/neis/data_services/ftp_files.html

@13 Jones, A.L. Dep. of Geological Sciences & Environmental Studies, State Univ. of New York

@14 Jones, R.H. Dep. of Preventive Medicine & Biometrics School of Medicine, Univ. of Colorado Health Sciences Center

@15 Normal Distribution by DoStat Company of both Webster West in the Dep. of Stat. at the Univ. of South Carolina & Todd Ogden in the Dep. of Biostat. at Columbia Univ.

<http://dostat.stat.sc.edu/prototype/calculators/index.php3?dist=Normal>

@16 The Central Weather Bureau of Taiwan

<http://www.cwb.gov.tw/V4e/index.htm>

@17 The Northern California Earthquake Data Center

<http://quake.geo.berkeley.edu/ncedc/>

@18 Earthquake Data Catalog of Univ. of Nevada

<http://quake.seismo.unr.edu/ftp/pub/catalog/>

@19 UN Office for the Coordination of Humanitarian Affairs (OCHA)

<http://www.reliefweb.int/w/rwb.nsf>